Analog Integr Circ Sig Process (2007) 53:119–128
DOI 10.1007/s10470-007-9067-3

SPECIAL SECTION ON DTIP 2006

A new formulation of fringing capacitance and its application to the control of parallel-plate electrostatic micro actuators

Mehran Hosseini · Guchuan Zhu · Yves-Alain Peter

Received: 30 June 2006 / Revised: 29 August 2006 / Accepted: 10 May 2007 / Published online: 27 June 2007

Abstract Though the effect of fringing field in electrostatic parallel-plate actuators is a well-understood phenomenon, the existing formulations often result in complicated mathematical models from which it is difficult to determine the deflection of the moving plate for given voltages and hence, they are not suitable for accurate actuation control. This work presents a new formulation for tackling the fringing field, in which the effect of fringing field is modeled as a variable serial capacitor. Based on this model, a robust control scheme is constructed using the theory of input-to-state stabilization (ISS) and backstepping state feedback design. This method allows loosening the stringent requirements on modeling accuracy without compromising the performance. The stability and the performance of the system using this control scheme are demonstrated through both stability analysis and numerical simulation.

Keywords Fringing field effect · Modeling of electrostatic MEMS · FEM based simulation · Input-to-state stabilization · Robust nonlinear control

M. Hosseini · Y.-A. Peter
Engineering Physics Department, École Polytechnique de Montréal, C.P. 6079, Succursale centre-ville, Montreal, QC, Canada H3C 3A7

G. Zhu (✉)
Electrical Engineering Department, École Polytechnique de Montréal, C.P. 6079, Succursale centre-ville, Montreal, QC, Canada H3C 3A7
e-mail: guchuan.zhu@polymtl.ca

1 Introduction

In the most popular model of electrostatic parallel-plate actuators, only the main electrical field (perpendicular to both electrodes) is considered and the capacitance of the structure is computed by

$$C = \epsilon WL/G, \tag{1}$$

where W and L are the width and the length of electrodes, respectively, G indicates the separation distance, and ϵ is the permittivity in the gap. This formulation leads to a simple model of parallel-plate devices, but it is not accurate when the gap size separating the electrodes is comparable to the geometrical extent of the plates. The capacitance of the structure including the effect of fringing field can be computed by Laplace formula (see, e.g., [1]). Although this formula can be used in finite element methods (FEM) and leads to very accurate estimation of the real values in a static manner, it is not susceptible to analytic calculations. Assuming zero thicknesses for the plates, several approximate analytical formulae have been developed for the capacitance in the presence of the fringing field, such as Palmer [1] and Elliot [2] models. A number of other formulae have also been recommended assuming finite thicknesses for the electrodes [3–8].

Although the recommended equations consider fringing field in the modeling of parallel-plate capacitors, these formulations provide only approximate expression and are not mathematically simple. In particular, these formulae are highly nonlinear and it is difficult to determine the deflection of the moving plate for a given capacitance. Therefore they are not suitable for predicting the applied voltages for actuation control.

In this work, we present a new method for the modeling of fringing capacitance, in which the effect of fringing field is considered as a variable serial capacitor. In general, the analytical expression of the serial capacitor in terms of deflections is not easy to determine. However, with an appropriate robust control scheme, the knowledge of the relationship between serial capacitance and deflection is not required, but merely its variation boundaries, which can be estimated by numerical simulation or experimental measurement. This method keeps the simplicity in the modeling while it is still possible to obtain the desired performance through the use of robust control techniques.

The proposed formulation can easily cope with other type of modeling errors, such as parallel parasitics and parametric uncertainties, thus it can be applied to the control of more generic MEMS devices. Note that the deformation of the moving plate and the singularity appearing at the corners and the edges of the structure will also introduce the deviation of the capacitance from the simplified model (1) [9, 10]. These modeling errors can also be handed by the method developed in this work.

The robust control scheme proposed in this work is based on the theory of input-to-state stabilization (ISS) and backstepping state feedback design [11, 12]. The nominal model used in control law design is the simplified parallel-plate actuator without fringing filed, but the controller is made robust against parasitics and parametric uncertainties. The stability and the performance of the system using this control scheme are demonstrated through both stability analysis and numerical simulation.

The rest of the paper is organized as follows. Section 2 models the capacitance of 1DOF parallel-plate electrostatic actuator with fringing field effect. In Section 3 the equation of motion of the device and the dynamics of the driving circuit are established. Section 4 is devoted to the construction of control law. The simulation results are reported in Section 5 and Section 6 contains some concluding remarks.

2 Modeling of fringing field

Consider the Palmer formula for the capacitance of a rectangular parallel-plate structure [1]:

$$C_f = \frac{\epsilon WL}{G}\left(1+\frac{G}{\pi W}\left(1+\ln\left(\frac{2\pi W}{G}\right)\right)\right) \times \left(1+\frac{G}{\pi L}\left(1+\ln\left(\frac{2\pi L}{G}\right)\right)\right). \quad (2)$$

As will be seen, this equation conforms to the simulation results to a great extent.

To present an image of the accuracy of different formulations, we consider a parallel-plate actuator with rectangular electrodes of 600 μm × 300 μm and an initial separation distance G_0 = 305 μm. Figure 1 shows the simulated capacitance of the device obtained by using FEM based CAD software CoventorWare™, presented as a function of the normalized deflection from the zero-voltage position. This result has been compared to the one given by the simplified expression (1) and the 2-D Palmer formula (2), respectively. As can be seen from Fig. 1, at the initial stage when gap is comparable to the dimensions of the electrodes, the simplified expression considerably underestimates the real value of the capacitance (about 35% of the real one). Decreasing the gap will attenuate the effect of fringing field and when both W/G and L/G become more than 100, the difference between the two becomes less than 5%. On the other hand, the 2-D Palmer formula gives a close approximation to the simulation results (6% of error for the initial gap, decreasing with gap reduction).

Clearly, the fringing field has the effect of increasing the capacitance and, consequently, the electrostatic force. It has to be noted that (as shown in Fig. 1) the extra capacitance due to the fringing field decreases as the gap closes. Therefore, we can use an over-estimated capacitor (which follows the simplified model (1)) combined with an appropriate variable serial capacitor to represent the total capacitance of the device.

Based on this idea, we developed a model for parallel-plate actuators, including a substitute capacitor, C_a, and a serial capacitor C_{sp}. The substitute capacitor is chosen to have the same capacitance as the real device at the zero voltage position, but to follow Eq. (1) instead, when the gap decreases. Obviously, to satisfy these conditions, the effective electrode areas of the substitute capacitor must be larger than the real one. The value of the introduced serial capacitor is a function of the gap and can be expressed as

$$\frac{1}{C_{sp}} = \frac{1}{C_{real}} - \frac{1}{C_a}, \quad (3)$$

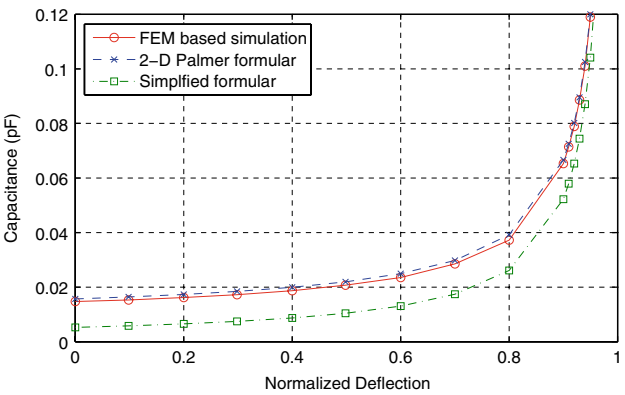

Fig. 1 Comparison of the simulation results with analytical formulae

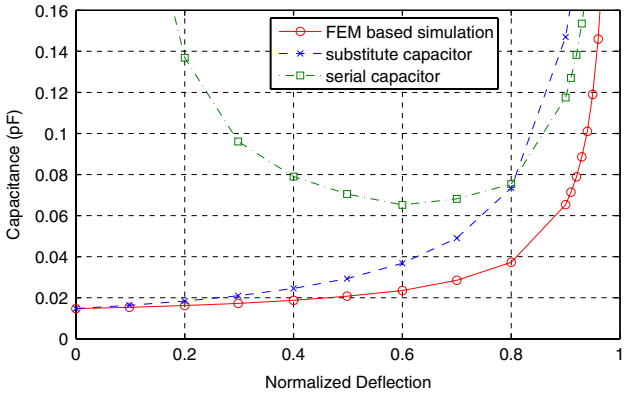

Fig. 2 Capacitances of the real (simulated) device, its substitute capacitor, and the introduced serial capacitor

where C_{real} is the real (or simulated) capacitance of the device. Obviously, since C_{real} is unknown, one can not determine C_{sp}. However, as mentioned earlier, for an appropriate robust control scheme, the full knowledge of the relationship between serial capacitance and deflection is not required, but merely its variation boundaries.

Figure 2 shows the capacitance of the simulated device, C_{real}, and the substitute capacitor, C_a. The introduced serial capacitor, C_{sp}, is computed from C_{real} and C_a using (3). The value of the substitute capacitor at the initial gap is equal to 1.47×10^{-2} pF (the same as the real capacitor at the same position). Except for the initial separation distance, there is a difference between the value of substitute capacitor and the real one. The role of the serial capacitor is to compensate this difference. As shown in Fig. 2, this serial capacitance is infinite at the initial gap and has a minimum that is about 6.47×10^{-2} pF for this structure. Since the smaller the introduced serial capacitance, the bigger the influence of modeling errors, we can use this value to determine the boundary of the introduced serial capacitor in the model. As the introduced serial capacitor is essentially unknown to the control scheme, it can be seen as serial parasitics.

Note that the simulation has been done for a rigid structure. For the case of a deformable structure, the procedure to determine the boundaries of serial parasitics will be the same.

3 Equation of motion and dynamics of driving circuit

The schematic representation of the device is shown in Fig. 3(a), in which G is the gap separating the two electrodes and G_0 is the zero voltage gap. Denote by Q_a the charge on the device and by A the plate area. The equation of motion of the parallel-plate actuator is then given by (see e.g. [13]):

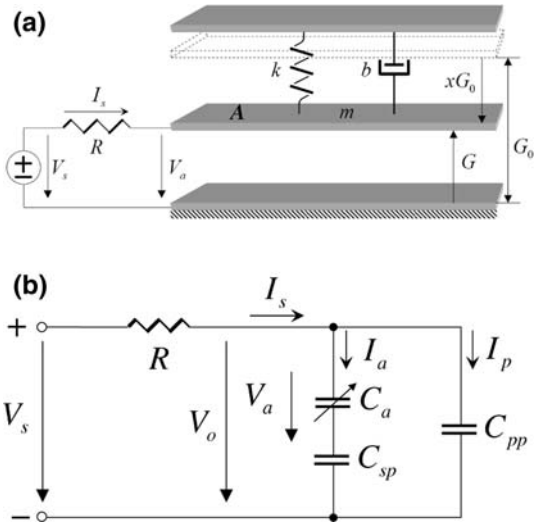

Fig. 3 1DOF parallel-plate electrostatic actuator with serial and parallel parasitic capacitances: (**a**) schematic representation; (**b**) equivalent circuit

$$m\ddot{G}(t) + b\dot{G}(t) + k(G(t) - G_0) = -\frac{Q_a^2(t)}{2\epsilon A}, \tag{4}$$

where m, b, and k are the mass of the moveable upper electrode, the damping coefficient, and the elastic constant, respectively.

In this work, the parallel parasitic capacitance, C_{pp}, due to e.g. the layout, is also considered. The equivalent circuit of the device driven by a voltage source is shown in Fig. 3(b). It is shown in Appendix A that the dynamic equation of the electrical subsystem in the presence of parasitics is given by

$$\begin{aligned}\dot{Q}_a(t) = &\frac{1}{R\left(1 + \rho_p\rho_s + \rho_p\dfrac{G}{G_0}\right)} \\ &\times \left(V_s - \left(\frac{G}{\epsilon A} + \rho_s\frac{G_0}{\epsilon A} + R\rho_p\frac{\dot{G}}{G_0}\right)Q_a\right),\end{aligned} \tag{5}$$

where I_S, V_S, and V_a are the source current, the applied voltage, and the actuation voltage, respectively, and

$$\rho_p = \frac{C_{pp}}{C_0}, \quad \rho_s = \frac{C_0}{C_{sp}},$$

with $C_0 = \varepsilon A/G_0$, the capacitance of the device corresponding to the initial gap G_0.

In our modeling, ρ_p and ρ_s represent the influence of parasitics. When their value is set to zero, the dynamics of the electrical subsystem will be reduced to the one for ideal devices.

It can be seen from (5) that the parallel parasitic capacitance will not change the static behavior of the device.

However, the dynamics of the electrical subsystem will be affected: the bigger the parallel parasitic capacitance, the slower the dynamics of the driving circuit. Consequently, the performance of the system will be degraded if the parallel parasitic capacitance is not taken into account in the design of the control system.

The serial parasitic capacitance will affect both the static and the dynamic behavior of the system. Figure 4 illustrates the normalized static position of a parallel-plate device with respect to ρ_s when the input equals 1 (the normalized nominal pull-in voltage). It can be seen that the static position varies with respect to the serial parasitic capacitance. For open-loop control schemes, ignoring serial parasitics may result in significant regulation errors if the simplified model (1) is used to predict the deflections of the device. In general, the serial parasitics will move the pull-in position beyond 1/3 of the full gap. This matches the observations reported in the literature (see, e.g. [14]).

Finally, to make the system analysis and control design easier, we transform (4) and (5) into normalized coordinates by changing the time scale, $\tau = \omega_0 t$, and performing a normalization as follows [15]:

$$x = 1 - \frac{G}{G_0},\ q = \frac{Q_a}{Q_{pi}},\ u = \frac{V_s}{V_{pi}},\ i = \frac{I_s}{V_{pi}\omega_0 C_0},\quad r = \omega_0 C_0 R, \tag{6}$$

where $V_{pi} = \sqrt{8kG_0^2/27C_0}$ is the nominal pull-in voltage, $Q_{pi} = \frac{3}{2}C_0 V_{pi}$ the nominal pull-in charge, $\omega_0 = \sqrt{k/m}$ the undamped natural frequency, and $\zeta = b/2m\omega_0$ the damping ratio. Note that in the normalized coordinates, $x = 0$ and $x = 1$ correspond to the zero-voltage position and the full gap deflection, respectively, and the pull-in happens at $x = 1/3$. Note also that x is negative if the upper plate moves beyond the zero-voltage position.

In the new coordinates, the dynamics of the electrical subsystem (5) can be written as

$$\dot{q}(t) = \frac{1}{r\left(1 + \rho_p(1-x) + \rho_p\rho_s\right)} \times \left(\frac{2}{3}u - (1-x)q - \rho_s q + r\rho_p \dot{x} q\right). \tag{7}$$

Let $x_1 = x$, $x_2 = v$, and $x_3 = q^2$. System (4)–(7) can then be written in the normalized coordinates as

$$\dot{x}_1 = x_2 \tag{8a}$$

$$\dot{x}_2 = -2\zeta x_2 - x_1 + \frac{1}{3}x_3 \tag{8b}$$

$$\dot{x}_3 = \beta\left(\frac{4\sqrt{x_3}}{3}u - 2(1-x_1)x_3 - 2\rho_s x_3 + 2r\rho_p x_2 x_3\right) \tag{8c}$$

where

$$\beta = \frac{1}{r\left(1 + \rho_p(1-x_1) + \rho_p\rho_s\right)} \tag{9}$$

is a function of deflection. System (8) is defined on the state space $\mathcal{X} = \left\{(x_1, x_2, x_3) \subset \mathbb{R}^3 \,|\, x_1 \le 1,\ x_3 \ge 0\right\}$.

Note that the considered actuator exhibits switching behavior. First of all, when the movable plate hits the fixed one ($x_1 = 1$), the dynamics of the mechanical subsystem collapse [16]. In addition, $q = 0$ ($x_3 = 0$) is a singular point at which System (8) is not linearly controllable (see, e.g., [16]). However, it is easy to see that the system is symmetric except for the sign of the charge. For simplicity, we ignore the contact dynamics and consider only the branch defined by (8c). Consequently, the stability property obtained through the proposed control will hold locally.

Since in what follows we deal only with normalized quantities, we can use t to denote the time and omit the qualifier ''normalized.''

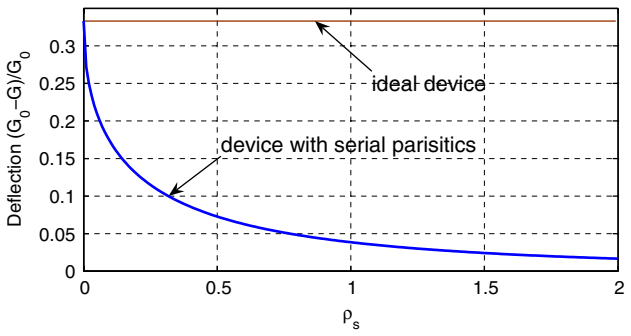

Fig. 4 Influence of serial parasitics to static behavior of parallel-plate devices

4 Control synthesis

4.1 Preliminaries of input-to-state stability

The concept of input-to-state stability is introduced by Sontag in [17] and ISS-based control system design is a popular tool in the field of system control. We present here only the notations required in the development of the control law. The interested reader is referred to, for example, [11, 12] for a formal presentation.

The following comparison functions are required for presenting the method of input-to-state stabilization. A function $\alpha : [0, a) \to [0, \infty)$ is said to belong to class-$\mathcal{K}$ if it is continuous, strictly increasing, and $\alpha(0) = 0$. If $a = \infty$ and α is unbounded, the function is said to belong to $\mathcal{K}_\infty$. A function $\beta : [0, a) \times [0, \infty) \to [0, \infty)$ is said to belong to $\mathcal{KL}$

if it is nondecreasing in its first argument, nonincreasing in its second argument, and $\lim_{s\to 0^+}\beta(s,t)=\lim_{t\to\infty}\beta(s,t)=0$.

The system

$$\dot{x}=f(x,u) \tag{10}$$

is said to be input-to-state stable if for any $x(0)$ and for any input $u(\cdot)$ continues and bounded on $[0,\infty)$ the solution exists for all $t\geq 0$ and satisfies

$$|x(t)|\leq \beta(x(0),t)+\gamma\left(\sup_{0\leq\tau\leq t}|u(\tau)|\right),\ \forall t\geq 0, \tag{11}$$

where $\beta(s,t)\in\mathcal{KL}$ and $\gamma(s)\in\mathcal{K}$.

A useful property of ISS that will be used in our control law design is that for a cascade of two systems

$$\dot{x}_1=f_1(x_1,x_2,u) \tag{12a}$$

$$\dot{x}_2=f_2(x_2,u) \tag{12b}$$

if the x_1-subsystem is ISS with respect to x_2 and u, and the x_2-subsystem is ISS with respect to u, then the cascade system is also ISS.

Note that the method of ISS provides a convenient framework for robust system control, which amounts to finding a control with which the closed-loop system is stable with respect to the disturbances, considered now as the inputs to the system.

4.2 Control synthesis

In this work, we consider both the parasitics and parametric uncertainties, such as the variations of damping coefficient and loop resistance. We make then the following assumptions on the uncertainties in System (8).

Assumption 1 The parasitic capacitances are bounded by known constants:

$$0\leq\rho_p\leq\bar{\rho}_p,\ \ 0\leq\rho_s\leq\bar{\rho}_s. \tag{13}$$

Assumption 2 The damping ratio is positive and bounded and can be written as:

$$\zeta=\zeta_0+\Delta\zeta, \tag{14}$$

where ζ_0 is positive-valued representing the nominal damping ratio and $\Delta\zeta$ the modeling error.

Assumption 3 The upper and lower bounds for the resistance r are known:

$$0<\underline{r}\leq r\leq\overline{r}. \tag{15}$$

Since $x_1\leq 1$, β in (9) may be bounded as follows:

$$0<\underline{\beta}\leq\beta\leq\overline{\beta}, \tag{16}$$

where $\overline{\beta}=1/\underline{r}$. Note that since the electrostatic force is always attractive, the control allowing the moveable plate to move as far as possible beyond the initial gap is the one that can remove the charge from the device in an arbitrary small time interval. However there is no equilibrium beyond the zero voltage gap and the mechanical subsystem (8-a)-(8-b) globally exponentially converges to the origin with zero input ($x_3=0$) [18]. This implies that the maximum amplitude of deflection beyond the zero voltage position (G_0 or $x_1=0$) should be bounded by $2G_0$, or $x_1\geq -1$, corresponding to a 100% of overshoot. Therefore, in a normal operational condition, β should be lower bounded by

$$\underline{\beta}=\frac{1}{\overline{r}\left(1+\overline{\rho}_p(2+\overline{\rho}_s)\right)}. \tag{17}$$

further more, the variation of β is denoted by

$$\Delta\beta\triangleq\beta-\beta_0, \tag{18}$$

where β_0 is the nominal value of β.

In this work, we will consider the tracking problem with $y=x_1$ as the output. Following a classical approach, we choose a sufficiently smooth reference trajectory y_r for x_1 as a function of time and then make this trajectory attractive.

A recursive procedure, called also backstepping design (see, e.g., [12] for a detailed presentation of this technique), is used in the design of the control law, which consists of, for System (8), the following three steps. The proof the ISS property of each subsystem is given in Appendix B.

Step 1. Consider the control of the subsystem (8a) with x_2 as the virtual input. Let $z_1=x_1-y_r$ be the position tracking error and choose the desired input (also called stabilizing function) as:

$$x_{2d}=\dot{y}_r-k_1z_1,\ \ k_1>0. \tag{19}$$

We will have then

$$\dot{z}_1=-k_1z_1+z_2, \tag{20}$$

where $z_2=x_2-x_{2d}$. It is easy to show that the tracking error z_1 satisfies

$$|z_1(t)|\leq|z_1(0)|e^{-\frac{1}{2}k_1t}+M\sup_{0\leq\tau\leq t}|z_2(\tau)|, \tag{21}$$

where M is a bounded positive number. Therefore System (20) is ISS if z_2 is continuous and uniformly bounded for any $k_1>0$.

Step 2. Differentiating now z_2 and taking into account (8), we have

$$\dot{z}_2 = \dot{x}_2 - \dot{x}_{2d} = -2\zeta x_2 - x_1 + \frac{1}{3}x_3 - \ddot{y}_r + k_1\dot{z}_1.$$

The stabilizing function for the subsystem (8a)-(8b) is chosen as

$$x_{3d} = 3(2\zeta_0 x_2 + x_1 + \dot{x}_{2d} - \kappa_2\zeta_0|x_2|z_2 - k_2 z_2). \tag{22}$$

With this control, the time derivative of z_2 becomes

$$\dot{z}_2 = -k_2 z_2 - 2\Delta\zeta x_2 - \kappa_2\zeta_0|x_2|z_2 + \frac{1}{3}z_3, \tag{23}$$

where $z_3 = x_3 - x_{3d}$.

Following the same idea presented in [19, 20], we can show that if Assumption 2 holds, $k_2 > 0$, $\kappa_2 > 0$, and z_3 is continuous and uniformly bounded, then

$$|z_2(t)| \le |z_2(0)|e^{-\frac{1}{2}k_2 t} + \sup_{0\le\tau\le t}\mu_2(\tau), \quad \forall t \ge 0, \tag{24}$$

where μ_2 is the following continuous and uniformly bounded function:

$$\mu_2 = \frac{2|\Delta\zeta x_2| + |z_3|/3}{k_2/2 + \kappa_2\zeta_0|x_2|}. \tag{25}$$

Therefore System (23) is ISS.

Step 3. The time derivative of x_{3d} along the solutions of (8) is given by

$$\dot{x}_{3d} = 3(ab_1 + b_2 - 2\Delta\zeta b_1 x_2), \tag{26}$$

where

$$\begin{aligned} a &= -2\zeta_0 x_2 - x_1 + \frac{1}{3}x_3,\\ b_1 &= 2\zeta_0 - k_1 - k_2 - \kappa_2\zeta_0(sgn(x_2)z_2 + |x_2|),\\ b_2 &= y_r^{(3)} + k_1\ddot{y}_r + (\kappa_2\zeta_0|x_2| + k_2)\dot{x}_{2d} + x_2. \end{aligned}$$

The dynamics of z_3 will then be given by:

$$\begin{aligned} \dot{z}_3(t) = \beta\left(\frac{4\sqrt{x_3}}{3}u - 2x_3(1-x_1) + 2r\rho_p x_2 x_3 - 2\rho_s x_3\right)\\ - 3(ab_1 + b_2 - 2\Delta\zeta b_1 x_2). \end{aligned} \tag{27}$$

Letting $U = \frac{4\sqrt{x_3}}{3}u$, the proposed controller for System (27) is given by:

$$\begin{aligned} U = 2x_3(1-x_1) + \frac{1}{\underline{\beta}}((3ab_1 + 3b_2 - k_3 z_3)\\ - \kappa_{31}\zeta_0|b_1 x_2|z_3 - \kappa_{32}(|ab_1 + b_2|)z_3\\ - \kappa_{33}\overline{r\rho}_p|x_2|x_3 z_3 - \kappa_{34}\overline{\rho}_s x_3 z_3). \end{aligned} \tag{28}$$

It can be shown that if Assumption 1–3 hold, $k_3 > 0$, $\kappa_{31} > 0$, $\kappa_{32} > 0$, $\kappa_{33} > 0$, and $\kappa_{34} > 0$, then System (27) with the backstepping controller (28) is ISS and

$$|z_3(t)| \le |z_3(0)|e^{-\frac{1}{2}k_3 t} + \sup_{0\le\tau\le t}\mu_3(\tau), \ \forall t \ge 0, \tag{29}$$

where μ_3 is the following continuous and uniformly bounded function:

$$\mu_3 = \mu_{31} + \mu_{32} + \mu_{33} + \mu_{34} \tag{30}$$

with

$$\mu_{31} = \frac{6|\Delta\zeta b_1 x_2|}{\frac{k_3}{8} + \frac{\beta}{\underline{\beta}}\kappa_{31}\zeta_0|b_1 x_2|}, \tag{31a}$$

$$\mu_{32} = \frac{3\frac{|\Delta\beta|}{\underline{\beta}}(|ab_1 + b_2|)}{\frac{k_3}{8} + \frac{\beta}{\underline{\beta}}\kappa_{32}(|ab_1 + b_2|)}, \tag{31b}$$

$$\mu_{33} = \frac{\frac{2\rho_p}{1+\rho_p(1+\rho_s)}|x_2|x_3}{\frac{k_3}{8} + \frac{\beta}{\underline{\beta}}\kappa_{33}\overline{r\rho}_p|x_2|x_3}, \tag{31c}$$

$$\mu_{34} = \frac{\frac{2\rho_s}{r(1+\rho_p(1+\rho_s))}x_3}{\frac{k_3}{8} + \frac{\beta\overline{\rho}_s}{\underline{\beta}}\kappa_{34}x_3}. \tag{31d}$$

(29) implies that z_3 should be bounded provided that the disturbances ($\Delta\zeta$, $\Delta\beta$, ρ_p, and ρ_s) are bounded, which in turn will guarantee the boundness of z_2 by virtue of (24). Hence, based on the property of cascade interconnected ISS systems, we can conclude that for System (8) and a sufficiently smooth reference trajectory y_r, if all the conditions declared in the design procedure hold, then the backstepping controller (28) renders the closed-loop error dynamics ISS. Furthermore, the ultimate bound for the tracking error z_1 can be rendered arbitrarily small by choosing the feedback gains k_1, k_2, and k_3, and the damping gain κ_2, κ_{31}, κ_{32}, κ_{33}, and κ_{34} large enough.

Note that the actual control u is singular when $x_3 = 0$. This is due to the uncontrollability of System (8) at the zero voltage position. However this situation happens only at this point. It is easy to see that System (8) is stabilizing at this position with an input $u = 0$. By defining an open ball $B_\varepsilon = \{X | \|X\| < \varepsilon\} \subset \mathcal{X}$ of radius ε centered at the origin, where $X = (x_1, x_2, x_3)^T$ and $|\cdot|$ the usual Euclidean norm, a more practical control law can be expressed as

$$u = \begin{cases} \dfrac{3}{4\sqrt{x_3}} U, & \text{for } X \notin B_\varepsilon \\ 0, & \text{for } X \in B_\varepsilon \end{cases} \tag{32}$$

where U is given by (28).

4.3 Reference trajectory design

In general, reference trajectories can be chosen to be any sufficiently smooth function $t \mapsto y(t)$, connecting the initial point at time t_i to a desired point at time t_f, such that the initial and final conditions are verified. The reference trajectory used in our control schemes is a polynomial of the following form:

$$y_r(t) = y(t_i) + (y(t_f) - y(t_i))\tau^5(t) \sum_{i=0}^{4} a_i \tau^i(t), \tag{33}$$

where $\tau(t) = (t - t_i)/(t_f - t_i)$. For a set-point control, the coefficients in (33) can be determined by imposing the initial and final conditions

$$\dot{y}(t_i) = \dot{y}(t_f) = \ddot{y}(t_i) = \ddot{y}(t_f) = y^{(3)}(t_i) = y^{(3)}(t_f) = 0,$$

which yield $a_0 = 126$, $a_1 = -420$, $a_2 = 540$, $a_3 = -315$, and $a_4 = 70$.

The polynomial in (33) is one of the most used reference trajectories in flatness based control. A more general formulation can be found in [21].

5 System simulation

In our simulation study, the parameters of the nominal plant are $\zeta_0 = 1$, $r_0 = 1$, $\rho_p = 0$, and $\rho_s = 0$. The actuator is supposed to be driven by a bipolar voltage source. The boundaries of parasitics and parametric uncertainties are fixed to be $\overline{\rho}_s = 2$, $\overline{\rho}_p = 5$, $\overline{r} = 2$, and $\underline{r} = 0.5$. We have then $\underline{\beta} = 0.0238$. Note that a small bias voltage is applied to the device in order to avoid the singularity at the origin.

Firstly we consider only the influence of the parasitics. Based on the simulation in Sect. 2 we have for the device considered $\rho_{s_{\max}} = 0.227$. In the simulation, we tested more important serial parasitics and introduced different level of parallel parasitics. It can be seen from Fig. 5 that in the simulated range of variation of the parasitics, the system performs nearly identically.

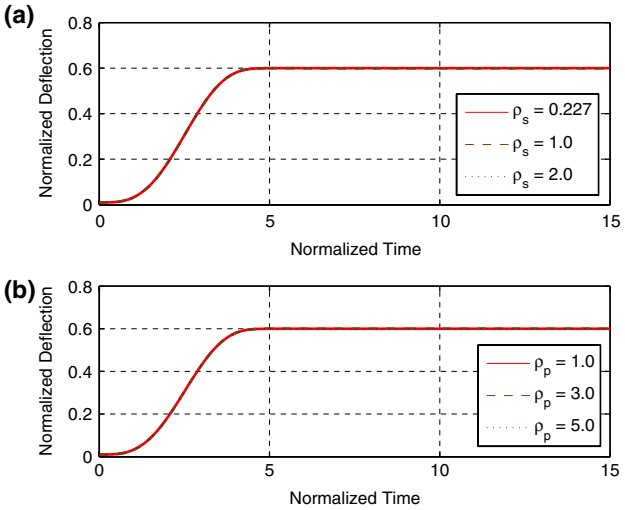

Fig. 5 Influence of parasitics: (**a**) variation of serial parasitics ρ_s; (**b**) variation of parallel parasitics ρ_p

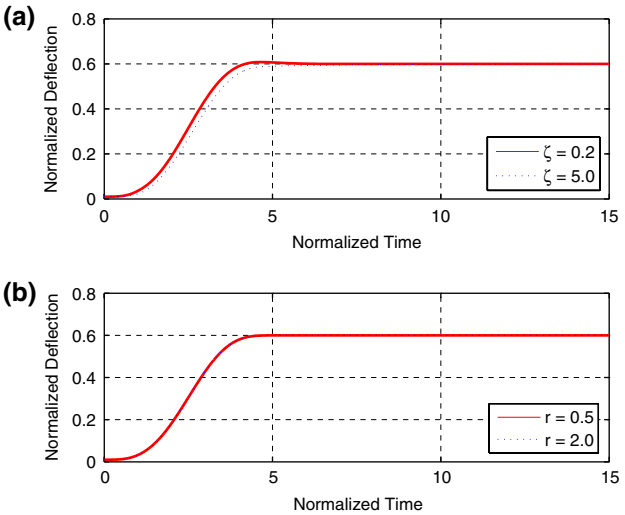

Fig. 6 Robustness against parametric uncertainties: (**a**) variation of damping coefficient ζ; (**b**) variation of resistance in the loop r

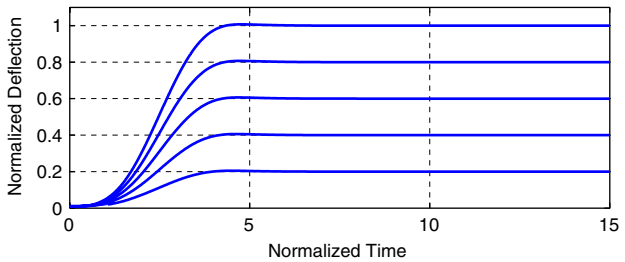

Fig. 7 Simulation results of set-point control

The second test is concerned with the uncertainties in the damping coefficient ζ and the resistance in the loop r. It is shown (see Fig. 6) that the system still performs very well even for very important parameter variations.

In the last test, we simulated the system for set-point control. The parameters for the simulated system are chosen as $\rho_s = 0.227$, $\rho_p = 1.0$, $\zeta = 0.5$, and $r = 1.5$. It can be seen from Fig. 7 that the performance of the system is quite uniform for different deflections.

6 Conclusions

This paper presents a new model of parallel-plate electrostatic micro-actuators in which the effect of fringing field is represented by a variable serial capacitor. The exact analytical expression of the serial capacitance is not required, but only its boundary represented by the ratio of its minimal value and the equivalent nominal capacitance at the initial position. FEM based software package ConventorWare™ was used to estimate the variation range of this serial capacitor. The dynamics of the driving circuits, which cope also with parallel parasitics have then been deduced. A state feedback robust control scheme is constructed and the closed-loop stability of the system is demonstrated using the technique of ISS. Numerical simulations show that the proposed control system has satisfactory performance and robustness vis-à-vis parasitics and parametric uncertainties. Since under the practical operational condition full state measurement may not be available, output feedback control should be more realistic. This issue is addressed in a separate work. Finally, we note that for torsional and multi-degree-of-freedom devices, it is vary difficult to model fringing field effect. Presenting this phenomenon by parasitics, using numerical simulation or experimental measurements to determine its boundaries, and then employing robust control techniques seem to be a very promising approach for devices with complex structure.

Appendix A: Modeling of electrostatic MEMS with parasitics

Denoting by Q_{pp} the charge on C_{pp} and applying Kirchhoff laws yields:

$$I_s R = V_s - V_0, \tag{A-1}$$

$$I_s = I_a + I_p = \dot{Q}_a + \dot{Q}_{pp}. \tag{A-2}$$

Since the voltage across the actuator is:

$$V_a = \frac{C_{sp}}{C_a + C_{sp}} V_o = \frac{Q_a}{C_a}, \tag{A-3}$$

it follows that:

$$\frac{Q_{pp}}{C_{pp}} = V_o = \frac{C_a + C_{sp}}{C_a C_{sp}} Q_a, \tag{A-4}$$

hence

$$Q_{pp} = \frac{C_{pp}(C_a + C_{sp})}{C_a C_{sp}} Q_a \tag{A-5}$$

and

$$\dot{Q}_{pp} = -\frac{C_{pp} Q_a}{C_a^2} \dot{C}_a + \frac{C_{pp}(C_a + C_{sp})}{C_a C_{sp}} \dot{Q}_a. \tag{A-6}$$

We can deduce from (A-1), (A-2), and (A-4) that

$$V_s - \frac{C_a + C_{sp}}{C_a C_{sp}} Q_a = R\left(\frac{C_a C_{sp} + C_{pp}(C_a + C_{sp})}{C_a C_{sp}} \dot{Q}_a - \frac{C_{pp} Q_a}{C_a^2} \dot{C}_a \right),$$

or equivalently

$$\dot{Q}_a(t) = \frac{C_a C_{sp}}{R(C_a C_{sp} + C_a C_{pp} + C_{sp} C_{pp})} \times \left(V_s - \left(\frac{C_a + C_{sp}}{C_a C_{sp}} - \frac{R C_{pp}}{C_a^2} \dot{C}_a \right) Q_a \right), \tag{A-7}$$

which can then be rewritten as (5).

Appendix B: ISS property of closed-loop error dynamics

From (23) we have

$$\begin{aligned} \frac{d}{dt}\frac{z_2^2}{2} &= z_2\left(-k_2 z_2 - 2\Delta\zeta x_2 - \kappa_2 \zeta_0 |x_2| z_2 + \frac{1}{3} z_3 \right) \\ &\le -\frac{k_2}{2} z_2^2 - \left(\frac{k_2}{2} + \kappa_2 \zeta_0 |x_2| \right) |z_2| \\ &\quad \times \left(|z_2| - \frac{2|\Delta\zeta x_2| + \frac{|z_3|}{3}}{\frac{k_2}{2} + \kappa_2 \zeta_0 |x_2|} \right) \\ &= -\frac{k_2}{2} z_2^2 - \left(\frac{k_2}{2} + \kappa_2 \zeta_0 |x_2| \right) |z_2| (|z_2| - \mu_2), \end{aligned} \tag{B-1}$$

where μ_2 is defined in (25). Since the numerator and the denominator of μ_2 grow with the same rate with respect to

$|x_2|$, μ_2 will be uniformly bounded if z_3 is uniformly bounded. Therefore we get for $|z_2| \geq \mu_2$ that

$$\frac{d}{dt}\frac{z_2^2}{2} \leq -k_2 z_2^2 \qquad (B-2)$$

and [12, 22]

$$|z_2(t)| \leq |z_2(0)|e^{-\frac{1}{2}k_2 t} + \sup_{0\leq\tau\leq t}\mu_2(\tau). \qquad (B-3)$$

Let's consider the time derivative of z_3^2. From (27) and (28) we have

$$\begin{aligned}\frac{d}{dt}\frac{z_3^2}{2} &= z_3(-3(ab_1+b_2-2\Delta\zeta b_2 x_2)\\ &\quad+\beta\left(\frac{3}{\underline{\beta}}\left(ab_1+b_2-\frac{k_3}{3}z_3\right)+2r\rho_p x_2 x_3\right.\\ &\quad-2\rho_s x_3-\frac{1}{\underline{\beta}}(\kappa_{31}\zeta_0|b_1x_2|z_3+\kappa_{32}(|ab_1+b_2|)z_3\\ &\quad\left.+\kappa_{33}\overline{r\rho}_p|x_2|x_3z_3+\kappa_{34}\overline{\rho}_s x_3 z_3)\right))\\ &\leq -k_3 z_3^2-6\Delta\zeta x_2 b_1-\frac{\beta}{\underline{\beta}}\kappa_{31}\zeta_0|b_1x_2|z_3^2\\ &\quad-3\left(\frac{\beta}{\underline{\beta}}-1\right)(ab_1+b_2)z_3-\frac{\beta}{\underline{\beta}}\kappa_{32}(|ab_1+b_2|)z_3^2\\ &\quad+2\beta r\rho_p x_2x_3z_3-\frac{\beta}{\underline{\beta}}\kappa_{33}\overline{r\rho}_p|x_2|x_3z_3^2-2\beta\rho_s x_3\\ &\quad-\frac{\beta\overline{\rho}_s}{\underline{\beta}}\kappa_{34}x_3z_3^2.\end{aligned}$$

We therefore have

$$\begin{aligned}\frac{d}{dt}\frac{z_3^2}{2} &\leq -\frac{k_3}{2}z_3^2\\ &\quad-\left(\frac{k_3}{8}+\frac{\beta}{\underline{\beta}}\kappa_{31}\zeta_0|b_1x_2|\right)|z_3|(|z_3|-\mu_{31})\\ &\quad-\left(\frac{k_3}{8}+\frac{\beta}{\underline{\beta}}\kappa_{32}(|ab_1+b_2|)\right)|z_3|(|z_3|-\mu_{32})\\ &\quad-\left(\frac{k_3}{8}+\frac{\beta}{\underline{\beta}}\kappa_{33}\overline{r\rho}_p|x_2|x_3\right)|z_3|(|z_3|-\mu_{33})\\ &\quad-\left(\frac{k_3}{8}+\frac{\beta\overline{\rho}_s}{\underline{\beta}}\kappa_{34}x_3\right)|z_3|(|z_3|-\mu_{34})\end{aligned} \qquad (B-4)$$

where μ_{31}, μ_{32}, μ_{33}, and μ_{34} are defined in (31). Since the numerator and the denominator in μ_{31}, μ_{32}, μ_{33}, and μ_{34} grow with the same rate with respect to the state variables, those functions are all uniformly bounded. Therefore we have for $|z_3| \geq \mu_3$ that

$$\frac{d}{dt}\frac{z_3^2}{2} \leq -k_3 z_3^2 \qquad (B-5)$$

and [12, 22]

$$|z_3(t)| \leq |z_3(0)|e^{-\frac{1}{2}k_3 t} + \sup_{0\leq\tau\leq t}\mu_3(\tau). \qquad (B-6)$$

References

1. Palmer, B. (1937). Capacitance of a parallel-plate capacitor by the Schwartz- Christoffel transformation. *Transactions on AIEE, 56*(3), 363–366.
2. Elliott, R. S. (1966). *Electromagnetics*. New York: McGraw-Hill.
3. Chang, W. H. (1977). Analytic IC-metal-line capacitance formulas. *IEEE Transactions on Microwave Theory and Techniques, MTT-24*(9), 608–611.
4. Yuan, C. P., & Trick, T. N. (1982). A simple formula for the estimation of the capacitance of two-dimensional interconnects in VLSI circuits. *IEEE Electron Device Letters, EDL-3*(12), 391–393.
5. Sakurai, T., & Tamaru, K. (1983). Simple formulas for two- and threedimensional capacitances. *IEEE Transactions on Electron Devices, ED- 30*(2), 183–185.
6. de Meijs, N. V., & Fokkema, J. T. (1984). VLSI circuit reconstruction from mask topology. *Integration, 2*(2), 85–119.
7. Yang, H. (2000). Microgyroscope and Microdynamics. Ph.D. Dissertation.
8. Sloggett, G. J., Barton, N. G., & Spencer, S. J. (1986). Fringing fields in disc capacitors. *Journal of Physics A: Mathematical and General, 19*, 2725–2736.
9. Chan, E., & Dutton, R. (2000). Electrostatic micromechanical actuator with extended range of travel. *Journal of Microelectromechanical Systems, 9*(3), 321–328, Spet.
10. Ong, E., Lee, K., & Lim, K. (2003). Singular elements for electromechanical coupling analysis of micro-devices. *Journal of Micromechanics and Microengineering, 13*, 57–68.
11. Sontag, E. (2000). The ISS philosophy as a unifying framework for stabilitylike behavior. In: A. Isidori, F. Lamnabhi-Lagarrigue, & W. Respondek (Eds.), *Nonlinear control in the year 2000 (Volume 2)*. ser. Lecture Notes in Control and Information Sciences, pp. 443–468. Berlin: Springer- Verlag.
12. Krstić, M., Kanellakopoulos, I., & Kokotović, P. (1995). *Nonlinear and Adaptative Control Design*. New York: John Wiley & Sons Ltd
13. Senturia, S. (2002). *Microsystem Design*. Norwell, MA: Kluwer Academic Publishers.
14. Cheng, J., Zhe, J., & Wu, X. (2004). Analytical and finite element model pull-in study of rigid and deformable electrostatic microactuators. *Journal of Micromechanics and Microengineering, 14*, 57–68.
15. Pont-Nin, J., Rodríguez, A., & Castañer, L. (2002). Voltage and pull-in time in current drive of electrostatic actuators. *Journal of Microelectromechanical Systems, 11*(3), 196–205.
16. Maithripala, D. H. S., Berg, J. M., & Dayawansa, W. P. (2005). Control of an electrostatic MEMS using static and dynamic output feedback. *ASME Journal of Dynamic Systems, Measurement and Control, 127*, 443–450.
17. Sontag, E. (1989). Smooth stabilization implies coprime factorization. *IEEE Transactions on Automatic Control, 34*, 435–443.

18. Maithripala, D., Berg, J., & Dayawansa, W. (2003). Nonlinear dynamic output feedback stabilization of electostatically actuated MEMS, in Proceedings of the 42nd IEEE Conference on Decision and Control, Maui, Hawaii, December 2003, pp. 61–66.
19. Yang, Z. -J., & Minashima, M. (2001). Robust nonlinear control of a feedback linearizable voltage-controlled magnetic levitation system. *Transactions of IEE of Japan, 121-C*(7), 1203–1211.
20. Zhu, G., Penet, J., & Saydy, L. (2006). Robust control of an electrostatic actuated MEMS in the presence of parasitics and parameter uncertainties, in Proc. of the 2006 American Control Conference, Minneapolis, Minnesota, June 14-16, pp. 1233–1238.
21. Lévine J. (2004). Analyse et Commande des Systmes Non Linaires. Online. Available: http://cas.ensmp.fr/%7Elevine/Enseignement /CoursENPC.pdf.
22. Krstić, M., Sun, J., & Kokotović, P. (1996). Robust control of nonlinear systems with input unmodeled dynamics. *IEEE Transactions on Automatic Control, 41*(6), 913–920.

Mehran Hosseini received the B.Sc. degree in electrical engineering in 1993 from Isfahan University of Technology (IUT), Isfahan, Iran, and the M.A.Sc. degree in electrical engineering 2005 from Concordia University, Montreal, Canada.

At the time of the submission of this work, he has been pursuing the Ph.D. degree in physics engineering in Ecole Polytechnique Montreal. He investigates Micro Electrical Mechanical Systems (MEMS) and his research focuses on modeling, simulation and fabrication of electro-statically actuated micro-mirrors.

Guchuan Zhu received the M.S. degree in electrical engineering from Beijing Institute of Aeronautics and Astronautics, China, the Ph.D. degree in mathematics and control from the École des Mines de Paris, France, and the graduate diploma in computer science from Concordia University, Montréal, Canada, in 1982, 1992, and 1999, respectively.

Prior to join the École Polytechnique de Montréal, Montréal, Canada, in 2004, where he is currently an Assistant Professor in the Department of Electrical Engineering, he worked as Lecturer in the Department of Electronic Engineering at Beijing Institute of Aeronautics and Astronautics, Postdoctoral Researcher and Research Fellow at the École de Technologie Supérieure, Montréal, Canada, and Software Designer at SR Telecom Inc., Montréal, Canada. Dr. Zhu's current research interests include nonlinear system control with applications to microsystems.

Yves-Alain Peter received the M.S. and Ph.D. degrees in physics from the University of Neuchâtet, Switzerland, in 1994 and 2001, respectively.

Currently, he is an Associate Professor and Scientific Director with the Laboratory for Microfabrication, Engineering Physics Department, Ecole Polytechnique de Montréal, Montréal, QC, Canada. In 1995, he was a Research Associate with the Medical Radiobiology Department, Paul Scherrer Institute, Switzerland. During 1995–2001, he was a Graduate Research Assistant with the applied optics group of the Institute of Microtechnology, University of Neuchâtel. From 2001 to 2003, he was a Postdoctoral Researcher with the microphotonics group at Stanford University, Stanford, CA. He was an R&D Engineer and Project Leader with the Swiss Center for Electronics and Microtechnology (CSEM), Switzerland, from 2003 to 2004. His research interests include micro and nano optoelectromechanical systems with applications in adaptive optics and tunable nanophotonics structures.

Dr. Peter is a member of IEEE/LEOS, OSA and the Swiss Physical Society.